Time reversal of optically carried radiofrequency signals in the microsecond range

Héloïse Linget, Loïc Morvan, Jean-Louis Le Gouët, Anne Louchet-Chauvet

Time-Reversal of Optically-carried Radiofrequency Signals in the Microsecond Range

H. Linget,[1,2] L. Morvan,[2] J.-L. Le Gouët[1] and A. Louchet-Chauvet[1]

[1] *Laboratoire Aimé Cotton, CNRS-UPR 3321, Bâtiment 505, 91405 Orsay, France*
[2] *Thales Research and Technology, avenue Fresnel, 91767 Palaiseau, France*

Compiled January 22, 2013

The time-reversal protocol we implement in an erbium doped YSO crystal is based on photon-echoes but avoids the storage of the signal to be processed. Unlike other approaches implying digitizing or highly dispersive optical fibers, the proposed scheme reaches the μs-range and potentially offers high bandwidth, both required for RADAR applications. In this letter, we demonstrate faithful reversal of arbitrary pulse sequences with 6 μs duration and 10 MHz bandwidth. To the best of our knowledge, this is the first demonstration of time reversal via linear filtering in a programmable material.

OCIS codes: 000.0000, 999.9999.

When a wave travels through an inhomogeneous medium, its wavefront is distorted by many phenomena, such as reflection, diffraction or anisotropy. Specifically velocity variations inside the medium distort the incident wavefront, and multireflection paths split it, resulting in a spatially and temporally poorly focused beam. Time-reversal (TR) invariance in the wave propagation equation can be used to counteract these effects. If a wave with time-varying amplitude *s(t)* propagates through a complex medium, the time-reversed waveform *s(-t)* is solution of the propagation equation too, but converges with accurate resolution back to the source responsible for the incident wave. Depending on the wavelength, different applications arise, from medicine with acoustic waves, to RAdio Detection And Ranging (RADAR) and electronic warfare devices with microwaves. Although digitizing the received signal *s(t)* is well-fitted to acoustic waves with limited bandwidth [1], the time-consuming analog-to-digital conversion excessively limits the bandwidth in the microwave domain (e.g. 2 MHz-wide TR in [2]). For broadband signals, pure analog approach is possible using optically carried RF signals. In this way, group delay dispersion (GDD) in optical fibers enables TR with 18 GHz bandwidth, but is not sufficiently large to process signals longer than few nanoseconds [3]. While GDD in an optical fiber is settled by its length, rare earth ion-doped crystals (REIC) at low temperature offer a group delay only limited by the homogeneous dephasing time T_2 of the doping ion, and almost 10^5 better than can be reached with km-long fibers. With these materials, we can thus extend the TR-processing to the μs-range required for RADAR applications, and possibly access 1-100 GHz bandwidth, limited by the inhomogeneous broadening of the transition. Three pulse photon-echo (3PE) in REIC has already been considered for TR [4], but the proposed procedure relied on the encoding of the RF signal in the active medium. To preserve the engraving linearity, one operates with low intensity pulses, which results in poor-contrast engraving and low processing efficiency [5]. In the present work, instead of storing the RF signal, we program a TR-specific function in the medium. This allows us to process differently shaped signals consecutively, after programming the crystal once and for all. Finally the non storing of the datas relaxes the low field condition, opening new ways to improve the programming step.

In a 3PE sequence at frequency ν_1, if the first two pulses are separated by $t_{12}^{(1)}$, the third one is followed by a $t_{12}^{(1)}$-delayed atomic emission [Fig.1(a,b)]. Considering that spectral classes are independently addressable in a REIC, we can reproduce this 3PE sequence at different frequencies $\{\nu_i\}$ with different durations $\{t_{12}^{(i)}\}$. As shown in figure 1(b), with a specific choice of parameters $\{\nu_i, t_{12}^{(i)}\}$, the sequence of all the third pulses (*time order : abcd*) is time-reversed in the echo (*time order : dcba*).

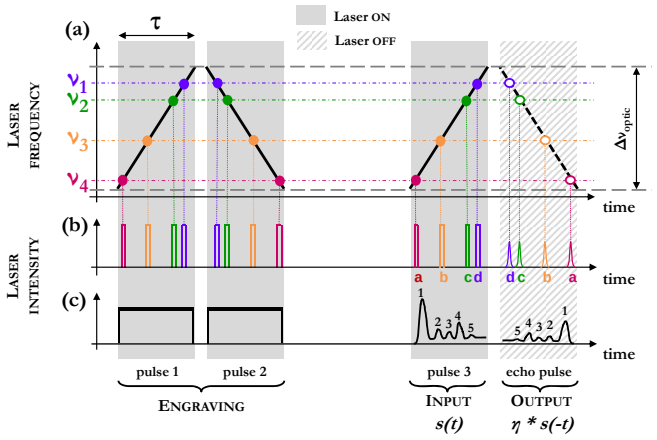

Fig. 1. (Color online) 3PE-scheme : (a) laser pulse (*solid line*) and echo (*dashed line*) chirped frequency, (b) 3PEs at 4 different frequency addresses, (c) TR protocol : continuous engraving is achieved by pulses 1 and 2. The waveform - carried by pulse 3 - is time reversed in the echo.

This step-by-step description can be extended to a continuous one by linearly chirping the laser frequency over a range $\Delta\nu_{optic}$ during a time τ. The monochromatic pulses of the 3PE are now replaced by three chirped pulses with respective rates $+r$, $-r$ and $+r$ where $r = \Delta\nu_{optic}/\tau$, resulting in an echo pulse with rate $-r$ [Fig.1(a)]. Since the photon echo signal intensity varies linearly with the third pulse intensity, the echo pulse is a time-reversed image of the input pulse with efficiency η.

Two monochromatic pulses separated by duration t_{12} engrave a grating with spectral spacing $1/t_{12}$ in the absorption profile. In our protocol, the spectral period of the grating engraved by chirped pulses 1 and 2 [Fig.2(a)] is frequency-dependent, varying as $1/t_{12}(\nu)$. It results in the encoding of a non-periodic structure over a range $\Delta\nu_{optic}$ as sketched in figure 2(b). It is important to notice that the time-reversal function is encoded by this non-periodic structure : the input pulse containing the signal will be processed by this function without being stored in the medium.

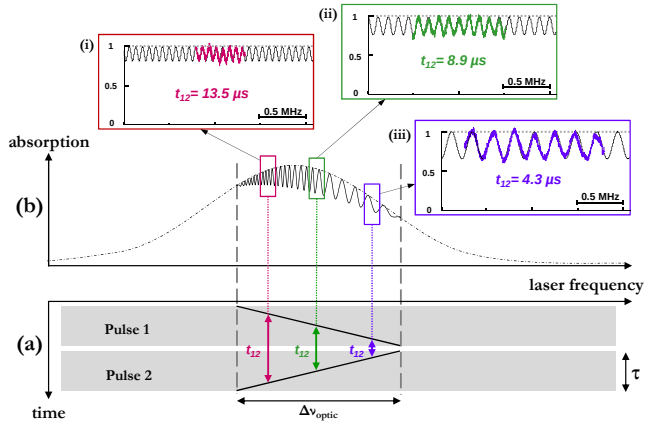

Fig. 2. (Color online) (a) frequency chirps during engraving, (b) schematic absorption profile, *dashed and solid line*: without and with engraving, (i)-(iii) normalized experimental transmission spectra, *black line* : sinusoidal fit. The maximum contrast reaches 15%.

The laser frequency is controlled by an electro-optic crystal inside the cavity [6]. A mode-hop-free tuning range $\Delta\nu_{optic}$ of 1,09 GHz in 6 μs can be reached ($r = 1.82 \cdot 10^{14} s^{-2}$). An acousto-optic modulator (AOM) is used to transpose the RF-signal *s(t)* on the chirped optical carrier during the input pulse. The laser beam propagates parallel to the *b* axis of a 10mm-long 0.005 % Er^{3+}:YSO crystal cooled at 1.7 K in a liquid helium cryostat, and is linearly polarized along the extinction axis D_2 of the crystal (strongest absorption of Er^{3+} substituted in site 1). To reduce spectral diffusion (SD), a 2-tesla magnetic field B is applied in the plane defined by the extinction axes (D_1, D_2) along direction $(B, D_1) \approx 135°$ [7]. The beam waist at the crystal has been adjusted to 65 μm, representing a trade-off between high-constrast grating and moderate instantaneous spectral diffusion [8]. To agree with RADAR specifications, the input signal duration lasts 6 μs, duration for which instantaneous spectral diffusion has a minor impact considering our experimental engraving power. The time-reversed output signal is finally detected by an avalanche photodiode (APD) placed after an AOM only opened during the echo pulse.

We have been able to time reverse a 6 μs asymmetric train of Gaussian pulses with a signal-to-noise ratio of 50 in single shot capture, only limited by the APD dynamic range. The 1.6‰ efficiency is consistent with the measured absorption profile modulation contrast [Fig.2(i)-(iii)]. The time-reversed waveform overall decay [Fig.3(b)] partly reflects the active ion interaction with a fluctuating environment [9]. This also results from the non-uniformity of the optical depth αL over the scanned range $\Delta\nu_{optic}$.

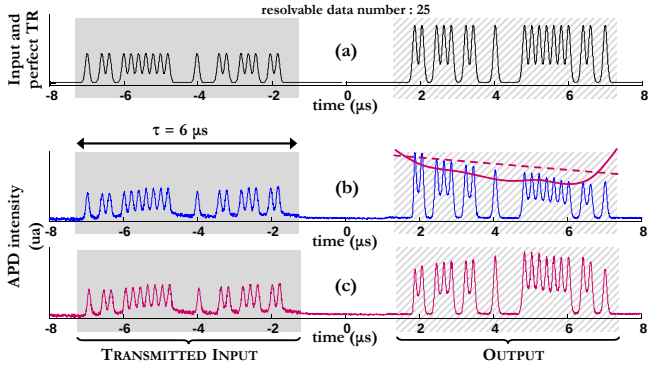

Fig. 3. (Color online) Input and output pulses : (a) input and perfectly time-reversed output, (b) single-shot experimental transmission, *red dashed line* : effect of interaction of Er^{3+} with fluctuating environment, *red solid line* : effect of optical depth variation over $\Delta\nu_{optic}$, (c) output corrected for the 2 previously cited effects.

At given frequency ν, input and output are separated by the group delay $\tau_g(\nu) = \tau_g(\nu_0) - 2(\nu - \nu_0)/r$. Let a Fourier transform limited, τ-long, temporal substructure be injected at frequency ν in the crystal. This pulse spreads over a spectral interval of order $1/\tau$. Due to group delay dispersion $\partial_\nu \tau_g(\nu) = -2/r$, the pulse undergoes temporal stretching of order $\partial_\nu \tau_g(\nu) \cdot 1/\tau = -2/(r\tau)$ while travelling through the crystal, and preserves its initial duration provided $\tau \gg |-2/(r\tau)|$. Hence, $\sqrt{2/r}$ represents the duration of the shortest temporal detail that can propagate throughout the medium without distortion. In other words, the processor bandwidth is limited to $\sqrt{r/2}$. In our experimental conditions, this limits RF bandwidth to approximately 10 MHz.

Knowing that the spectrum of a sequence of gaussian pulses of duration t_{gauss} is contained in a gaussian envelope of spectral width $1/(\pi \cdot t_{gauss})$, we can test this bandwidth by decreasing the parameter t_{gauss} of the input pulse, and thus broadening its spectral width $\Delta\nu_{RF}$. On the output pulse shown in figure 4(a), we notice the progressive appearance in *(ii)* and *(iii)* of unwanted oscillations due to the distortion of short temporal sub-

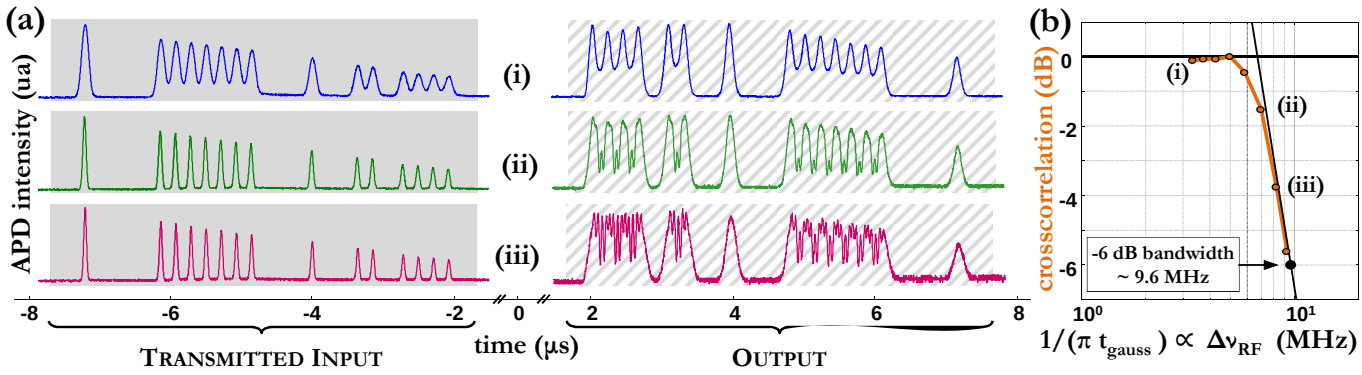

Fig. 4. (Color online) (a) Normalized input and output pulses for several gaussian pulse durations t_{gauss}. Output corrected for interaction with environment and αL-variation, (i) t_{gauss}=95ns, (ii) t_{gauss}=46ns, (iii) t_{gauss}=39ns, (b) Bode diagram representing normalized crosscorrelation between input pulse and time-reversed output pulse vs. input spectral bandwidth $\Delta\nu_{RF}$. Input intensity envelope modulations are due to αL-variation over the scanned range $\Delta\nu_{optic}$.

structures, as mentioned above. The faithfulness of the TR process has been quantified for several values of input spectral width using crosscorrelation between transmitted input and time-reversed output [Fig.4(b)]. It allows us to define a -6dB bandwidth of 9.6 MHz for our protocol, in agreement with the previously mentioned bandwidth. Our engraved TR-function is thus able to faithfully process frequencies lower than $\sqrt{r/2}$, but distortion occurs for higher spectral components.

In summary we have demonstrated a new time-reversal protocol dealing with signals up to the μs-range required for RADAR applications. Since the efficiency η of the process is proportional to the grating contrast squared, we can potentially increase our experimental value 1.6 ‰ (to be compared with 0.02 ‰, observed in [5]) by improving the absorption profile engraving. As the low-field regime is no longer required , we can imagine techniques other than photon-echo to achieve it, in a similar approach to the one considered for efficiency optimization of Atomic Frequency Comb engraving [10]. The limited bandwidth issue can be addressed in the framework of time-space duality. Indeed, true temporal imaging combines a temporal lens with two dispersive lines, respectively located upstream and downstream from the lens. These elements are needed to conjugate the temporal object and its time-reversed image [11, 12]. In our setup, where the chirped carrier and the programmed crystal respectively play the role of the lens and one dispersive line, the upstream dispersive element is missing, resulting in an approximate but simplified temporal imaging [13]. As a consequence, the *s(t)* time-reversed image is blurred, which is reflected in the bandwidth limitation. Double pass through the same programmed crystal could provide the two dispersion steps. However the processing efficiency is presently too weak for double pass operation. With improved efficiency, true temporal imaging could be implemented, taking full advantage of the crystal bandwidth. Finally it can be noticed that our system is the approximate temporal equivalent of an optical device called *camera obscura* (literally *dark chamber*) which recently gave rise to a heated debate within the Art history community about its assumed use by several famous Renaissance painters like Caravaggio or Vermeer [14].

This research received funding from the People Programme (Marie Curie Actions) of the European Union's Seventh Framework Programme FP7/2007-2013/ (REA grant agreement no. 287252).

References

1. M. Fink, Phys. Today **50**, 34 (1997).
2. G. Lerosey, J. De Rosny, A. Tourin, A. Derode, G. Montaldo, and M. Fink, Phys. Rev. Lett. **92**, 193904 (2004).
3. F. Coppinger, A. Bhushan, and B. Jalali, Electron. Lett. **35**, 1230 (1999).
4. T. Mossberg, Optics letters **7**, 77 (1982).
5. T. Wang, H. Lin, and T. Mossberg, Opt. Lett. **20**, 2033 (1995).
6. L. Ménager, L. Cabaret, I. Lorgeré, and J.-L. Le Gouët, Opt. Lett. **25**, 1246 (2000).
7. T. Böttger, C. Thiel, R. Cone, and Y. Sun, Physical Review B **79**, 115104 (2009).
8. G. Liu and R. Cone, Phys. Rev. B **41**, 6193 (1990).
9. T. Böttger, C. Thiel, Y. Sun, and R. Cone, Phys. Rev. B **73**, 075101 (2006).
10. M. Bonarota, J. Ruggiero, J.-L. Le Gouët, and T. Chanelière, Phys. Rev. A **81**, 033803 (2010).
11. C. Bennett, R. Scott, and B. Kolner, Appl. Phys. Lett. **65**, 2513 (1994).
12. M. Foster, R. Salem, Y. Okawachi, A. Turner-Foster, M. Lipson, and A. Gaeta, Nature Photonics **3**, 581 (2009).
13. J. Azaña, N. Berger, B. Levit, and B. Fischer, Photonics Technology Letters, IEEE **17**, 94 (2005).
14. M. Kemp, Max-Planck Institute für Wissenschaftsgeschichte pp. 243–264 (2007).

Informational Fourth Page

References

1. M. Fink, "Time reversed Acoustics", Physics Today, **20,**34–40 (1997).
2. G. Lerosey, J. De Rosny, A. Tourin, A. Derode, G. Montaldo, and M. Fink,"Time Reversal of Electromagnetic Waves", Phys. Rev. Lett. **92,** 193904 (2004).
3. F. Coppinger, A. Bhushan, and B. Jalali, "Time reversal of broadband microwave signals", Electron. Lett. **35,** 1230–1232 (1999).
4. T. Mossberg, "Time-domain frequency-selective optical data storage", Opt. Lett. **7,** 77–79 (1982).
5. T. Wang, H. Lin, and T. Mossberg, "Optical bit-rate conversion and bit-stream time reversal by the use of swept-carrier frequency-selective optical data storage techniques", Opt. Lett. **20,** 2033–2035 (1995).
6. L. Ménager and L. Cabaret and I. Lorgeré and J.-L. Le Gouët, "Diode laser extended cavity for broad-range fast ramping", Opt. Lett. **25,** 1246–1248 (2000).
7. T. Böttger, C . Thiel, R. Cone, and Y. Sun, "Effects of magnetic field orientation on optical decoherence in $Er^{3+} : Y_2SiO_5$", Phys. Rev. B **79,** 115104 (2009).
8. G. Liu and R. Cone, "Laser-induced instantaneous spectral diffusion in Tb^{3+} compounds as observed in photon-echo experiments", Phys. Rev. B **41,** 6193–6200 (1990).
9. T. Böttger, C. Thiel, Y. Sun, and R. Cone, "Optical decoherence and spectral diffusion at 1.5 μm in $Er^{3+} : Y_2SiO_5$ versus magnetic field, temperature, and Er^{3+} concentration", Phys. Rev. B **73,** 075101 (2006).
10. M. Bonarota, J. Ruggiero, J.-L. Le Gouët, and T. Chanelière, "Efficiency optimization for atomic frequency comb storage", Phys. Rev. A **81,** 033803 (2010).
11. C. Bennett, R. Scott, and B. Kolner, "Temporal magnification and reversal of 100 Gb/s optical data with an up-conversion time microscope ", Appl. Phys. Lett. **65,** 2513–2515 (1994).
12. M. Foster, R. Salem, Y. Okawachi, A. Turner-Foster, M. Lipson, and A. Gaeta, "Ultrafast waveform compression using a time-domain telescope", Nature Photonics **3,** 581–585 (2009).
13. J. Azaña, N. Berger, B. Levit, and B. Fisher, "Simplified temporal imaging systems for optical waveforms", Photonics Technology Letters, IEEE **17,** 94–96 (2005).
14. M. Kemp, "Inside the Camera Obscura: Optics and art under the spell of the projected image", W. Lefévre, ed., pp. 243–264 Max-Planck-Institute für Wissenschaftsgeschichte, Berlin, Germany, 2007.